J Mater Sci (2009) 44:2548–2552
DOI 10.1007/s10853-009-3332-z

Photocatalytic activities of $LaFe_{1-x}Zn_xO_3$ nanocrystals prepared by sol–gel auto-combustion method

Shuhua Dong · Kejing Xu · Guishan Tian

Received: 29 November 2008 / Accepted: 9 February 2009 / Published online: 5 March 2009

Abstract Nanophotocatalysts $LaFe_{1-x}Zn_xO_3$ ($x = 0, 0.05, 0.1, 0.3, 0.5$) were successfully prepared by sol–gel auto-combustion method. The samples were characterized by X-ray diffraction (XRD), ultraviolet/visible absorption spectra (UV–vis), scanning electron microscopy (SEM), and transmission electron microscopy (TEM). The photocatalytic activities of the prepared samples were investigated for the photodegradation of methylene blue (MB). The results show that the lattice constant of $LaFe_{1-x}Zn_xO_3$ nanocrystals increases due to the substitution of Zn for Fe, which leads to the lattice distortion. The absorption edges of Zn-doped $LaFeO_3$ display a red shift with a significant absorption between 400 and 500 nm. Doping with the Zn ions enhances the photodegradation rate of $LaFeO_3$ for MB. The $LaFe_{0.7}Zn_{0.3}O_3$ particles are spherical with mean grain size of about 20–30 nm, which exhibits the highest degradation rate of 75% under irradiation time of 150 min.

Introduction

Perovskite-type rare earth compound oxides such as ABO_3 are very important inorganic functional materials. To solve the questions of energy shortage and environment pollution, these compound oxides have recently been the focus in the fields of photocatalysis and photoelectricity conversion [1–3]. In the structure of ABO_3 perovskite, A is often alkaline-earth metal elements or rare earth elements while B is transition-metal elements. Cation B locates in octahedral vacancy and cation A fills the 12 coordinate cavities to form BO_6 network [4]. The energy level of ABO_3 perovskite (often less than 3.0 eV) is narrow, which can be easily excited under visible light or UV light irradiation [5]. Niu [6] has investigated systemically the photocatalytic activities of $REFeO_3$ (RE = Sm, Eu, Gd) for the degradation of various water-soluble dyes. A or B in the structure of ABO_3 can be replaced by doping some metal ions with the similar radius to maintain the crystal structure, and the formed polycomponent compound oxides possess some special physical and chemical properties [7]. Porob et al. [8] reported that La-doped $NaTaO_3$ perovskite-type solid exhibited higher photocatalytic activities than non-doped $NaTaO_3$, which was attributed to the particle morphology and fairly rough surface features. In our previous work, the photocatalytic activities of A site Sr-substituted $LaFeO_3$ and $LaMnO_3$ have been studied by citric acid complex method, respectively [9, 10].

Perovskite nanomaterials are often prepared by sol–gel [11], hydrothermal [12], and solid phase [13] methods. In this work, nanosize $LaFe_{1-x}Zn_xO_3$ ($x = 0, 0.05, 0.1, 0.3, 0.5$)particles were synthesized by sol–gel auto-combustion method. Sol–gel auto-combustion method, combining the advantages of sol–gel and self-propagating combustion method, is a kind of redox reaction of thermal induction anion using carboxylic acid ion as reductant and nitrate ion as oxidant. It has the advantages of low synthesis temperature, simply processing, easily operating, and uniformly mixing at the molecular/atomic level, obtaining powders with high purity and good uniformity [14–16].

In this study, high photocatalytic activity of B site doping $LaFeO_3$ nanoparticles was obtained by sol–gel auto-combustion method. The structure and the photocatalytic

S. Dong (✉) · K. Xu · G. Tian
Department of Materials Science and Engineering, Shandong University of Technology, Zibo 255049, People's Republic of China
e-mail: singer_dong@126.com

activities of $LaFe_{1-x}Zn_xO_3$ ($x = 0$, 0.05, 0.1, 0.3, 0.5) nanocrystals were investigated.

Experimental

Synthesis of photocatalysts

$LaFe_{1-x}Zn_xO_3$ samples were prepared by sol–gel auto-combustion method. Zinc nitrate [$Zn(NO_3)_2 \cdot 6H_2O$], lanthanum nitrate [$La(NO_3)_3 \cdot 6H_2O$], and ferric nitrate [$Fe(NO_3)_3 \cdot 9H_2O$] with molar ratio of $1:1 - x:x$ ($x = 0$, 0.05, 0.1, 0.3, 0.5) were dissolved in de-ionized water as A solution. Citric acid and ethylene glycol mixtures, mixed in 1:1 molar ratio, were dissolved in a right amount of de-ionized water and stirred for 10 min as B solution. B solution was added dropwise into A solution under vigorous magnetic stirring at 80 °C for 30 min. A violet red transparent solution was formed. The solution gradually became viscous with continuous stirring for 2.5 h until the amorphous gel formed. Then the gel was dried in an oven at 210 °C for 4 h. The dried gel was burnt in a self-propagating combustion manner and gave out a great deal of smoke and gases. Finally, all the gel was burnt out completely to form the fluffy loose burnt ashes. The resultant was further calcined at 750 °C for 1 h for better crystallization and homogeneous cation distribution in the space [17].

Characterization

The powder X-ray diffraction (XRD) patterns were recorded by an X-ray diffractometer (D8 ADVANCE, produced by Germany Brucker AXS Int.) using a Cu Kα radiation ($\lambda = 1.5406$ Å) at 40 kV and 40 mA. The average crystallite size of prepared powders was determined by using XRD patterns and Williamson-Hall approach. Pure Si is used as a standard reference material to correct the instrumental broadening. Kalpha2 and background were stripped out by MDI Jade 5.0 version. The morphology of the nanopowders was analyzed by a field emission scanning electron microscope (FEI SIRION 200) and a transmission electron microscope (Philips CM-30). BET surface area was measured by a nitrogen adsorption analyzer (NOVA300) at liquid nitrogen temperature. The ultraviolet/visible absorption spectra (UV–Vis) were measured by ultraviolet and visible spectrophotometer (China, WIN-Sp5).

Photocatalytic activity

In order to evaluate photocatalytic activity of the prepared samples, photodegradation rate of methylene blue (MB) was performed. The photocatalytic performance of the samples was determined by the 722 spectrophotometer at 664 nm (λ_{max} for MB) at a set time. A total of 100 mg of the prepared $LaFe_{1-x}Zn_xO_3$ nanocrystals was added into 200 mL methylene blue (MB) solution with a concentration of 5 mg/L. The MB solution was mixed by magnetic stirrer in dark for 2 h to establish absorption and desorption equilibrium. A 125 W high-pressure lamp ($\lambda_{max} = 365$ nm) was used as light source. Then, the light was turned on to begin illuminating. The mixed solution was taken out to filtrate by centrifugal filtration. We extracted the clear liquid to measure absorbance of methylene blue solution every 30 min. The degradation rate is calculated by the following formula: degradation rate (%) $= (A_0 - A)/A_0$, where A_0 represents the initial absorbance, while A the variable absorbance.

Results and discussion

XRD measurements

Figure 1 shows the XRD patterns of $LaFe_{1-x}Zn_xO_3$ ($x = 0$, 0.05, 0.1, 0.3, 0.5) samples calcined at 750 °C for 1 h. From these XRD results, the sharp peaks in the XRD patterns indicated well crystallinity of the prepared samples. The characteristic peaks of the samples are consistent with those in JCPDS No.75-0541 and no other diffraction peaks can be detected when x is less than 0.3, suggesting that the products are simple perovskite-type compound oxides. The crystal structure belongs to the cubic lattice with space group of *Pm3m* (221). However, there are new diffraction peaks from the impurity of $ZnFe_2O_4$ with cubic lattice (JCPDS No.82-1049) when $x = 0.5$, which is attributed to the difference in ionic radius between Zn^{2+}

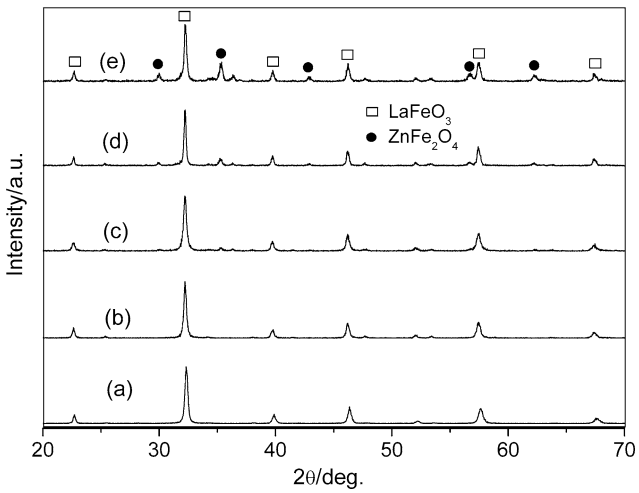

Fig. 1 X-ray diffraction (XRD) patterns of $LaFe_{1-x}Zn_xO_3$ samples with $x =$ (a) 0, (b) 0.05, (c) 0.1, (d) 0.3, (e) 0.5

($r_1 = 0.074$ nm) and Fe^{3+} ($r_2 = 0.064$ nm). $\Delta = [(r_1 - r_2)/r_1] \times 100\% = 13.5\% < 15\%$ [18], provides evidence for the formation of a finite solid solution with the substitution of Zn for Fe. This observation reveals that the nanocrystal Zn-doped $LaFeO_3$ powders can be synthesized directly by the auto-combustion method.

Crystallite size is determined using the Williamson-Hall formula, which is expressed as follows [19]:

$$B\cos\theta = \frac{k\lambda}{D} + 4\varepsilon\sin\theta \quad (1)$$

where B is the full-width at half maximum intensity, λ is the X-ray wavelength ($\lambda = 0.15406$ nm), θ is the diffraction angle, k is Scherrer constant, D is the average crystallite size (nm), and ε is the lattice strain. By plotting B $\cos\theta$ against 4 $\sin\theta$, the slope of the fitted linear regression line directly gives the lattice strain value (ε), while the crystallite size (D) can be calculated from the intercept of the line.

Table 1 gives the lattice parameter, crystal size, and specific surface area of $LaFe_{1-x}Zn_xO_3$ powder treated at 750 °C for 1 h. The lattice parameter a and the cell volume of Zn-doped $LaFeO_3$ increase, while the size decreases by comparison with the pure $LaFeO_3$. In the structure of $LaFeO_3$ that we investigated, since radius of Zn is similar to that of alkaline earth cation Fe, Zn^{2+} ions should enter into the lattice structure of $LaFeO_3$ to substitute the position of Fe ions under such a moderate temperature condition. As a result, the lattice expansion increases with the increase of Zn content and the tendency of grain growth will be inhibited by Zn ions. Zhang et al. [20] have demonstrated that Eu^{3+} substitutes the location of alkaline earth ions in the structure of $AZrO_3$, and the symmetry around Eu^{3+} ions is the same as that of the A^{2+} ions. As seen from Table 1, the smaller the crystallite size, the larger is the surface area. Large specific surface area is favorable for the improvement of photocatalytic activity.

SEM and TEM measurements

Figure 2 shows the SEM, TEM images, and electron diffraction (ED) pattern of the $LaFe_{0.7}Zn_{0.3}O_3$ after calcination at 750 °C for 1 h. It can be observed that the nanoparticles have a spherical morphology. The particles connect with each other to form a large network system with irregular sizes and shapes (Fig. 2a), due to the large number of escaping gases from the rapid decomposition of organic compounds and the strong redox reaction during sol–gel auto-combustion. The pore structure is favorable

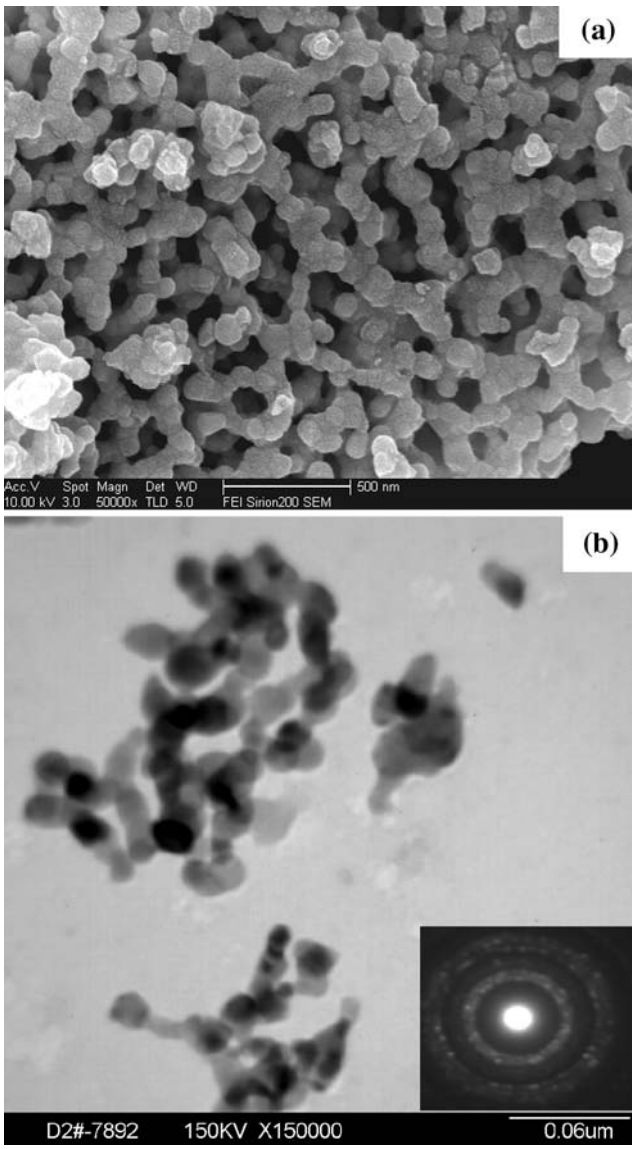

Fig. 2 SEM, TEM images, and electron diffraction (ED) pattern of $LaFe_{0.7}Zn_{0.3}O_3$ sample **a** SEM image, **b** TEM image and electron diffraction (ED) pattern

Table 1 Lattice parameter, crystal size, and specific surface area of $LaFe_{1-x}Zn_xO_3$ powder treated at 750 °C for 1 h

x value	a (nm)	Volume of crystal cell (nm^3)	Crystal size (nm)	Specific surface area ($m^2\ g^{-1}$)
0	0.3926	0.06051	50.22	66.02
0.05	0.3932	0.06079	43.95	72.56
0.1	0.3938	0.06107	37.06	73.08
0.3	0.3941	0.06121	28.33	76.87
0.5	0.3943	0.06130	33.77	76.04

for increasing the surface area of the powders and improving the photocatalytic activity [21], which suggests that sol–gel auto-combustion technology has superiority in preparing the perovskite-type nanocrystal. The image of TEM indicates that the particles are spherical with mean grain size of about 20–30 nm (Fig. 2b). The ED patterns confirmed that the sample has higher crystallinity.

UV–Vis spectroscopy

Figure 3 shows UV–vis spectra of the prepared samples. The absorption edges of Zn-doped $LaFeO_3$ display a red shift with a significant absorption between 400 and 500 nm, while pure $LaFeO_3$ had no absorption in the visible region (>400 nm). Replacing Fe^{3+} with Zn^{2+} will result in the formation of oxygen vacancies and additional energy levels, which make the average atomic distance increase and the energy gap decrease. As reported by Huang et al. [22], the narrower band gap of the semiconductor can harvest more photons to excite the electron from the valence band to the conduction band. Further enhanced visible light absorption ability is favorable for the improvement of the photocatalytic activity.

Photocatalytic activity

Figure 4 shows the photocatalytic degradation of the samples over different irradiation times. It can be seen that the degradation rate of methylene blue increases with the illumination time in the presence of photocatalysts, and the doping concentration of Zn has a great effect on degradation of MB solution. The photocatalytic activities of Zn-doped $LaFeO_3$ samples are advantageous over that of the undoped $LaFeO_3$. Figure 5 shows the effect of Zn doping concentration on the photocatalytic degradation for MB under the same time of 150 min. From the results, the order of photocatalytic

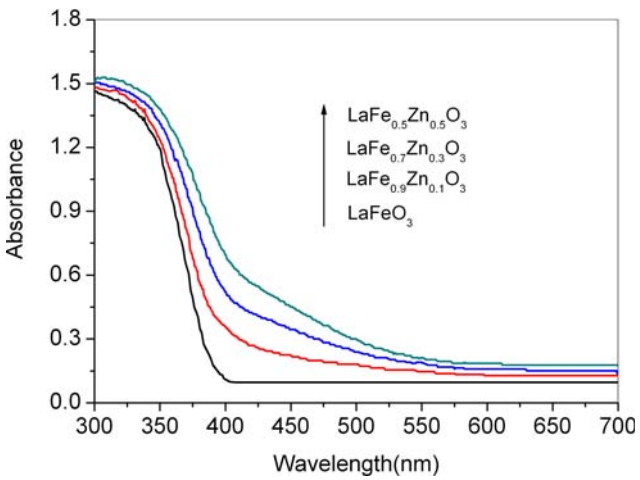

Fig. 3 UV–Vis absorption spectra of $LaFe_{1-x}Zn_xO_3$ samples

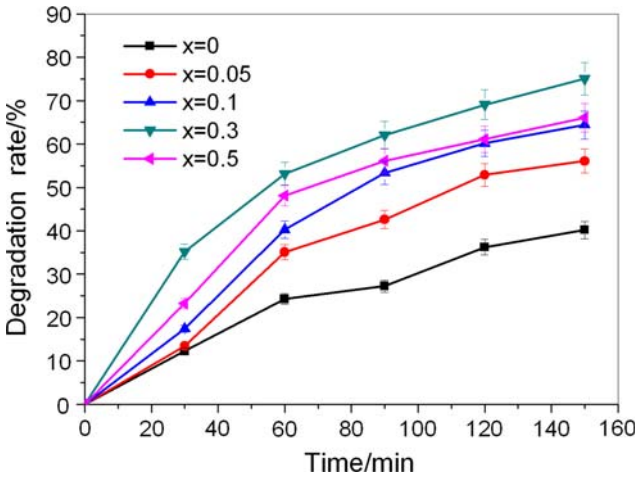

Fig. 4 Photocatalytic degradation curves of methylene blue over different irradiation times of $LaFe_{1-x}Zn_xO_3$ nanoparticles calcined at 750 °C for 1 h

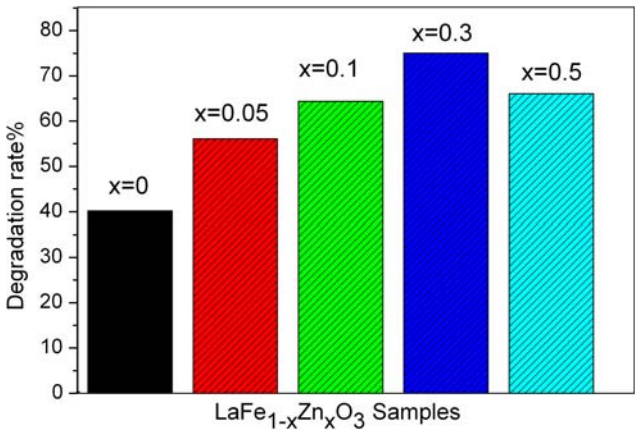

Fig. 5 Effect of Zn^{2+} doping amount on the photocatalytic degradation of the MB solution for light time of 150 min

activity of Zn-doped $LaFeO_3$ nanoparticles was as following: $LaFe_{0.7}Zn_{0.3}O_3 > LaFe_{0.5}Zn_{0.5}O_3 > LaFe_{0.9}Zn_{0.1}O_3 > LaFe_{0.95}Zn_{0.05}O_3 > LaFeO_3$. $LaFe_{0.7}Zn_{0.3}O_3$ sample shows the highest activity and degradation rate reaches 75%, which exceeds 35% compared with the $LaFeO_3$ as the catalyst.

It is known that the doped metal ion serves as an electron (e^-) trapper and prohibits the recombination of hole (h^+) and electron (e^-) pairs at low concentration. In addition, there are other reasons as fellows. First, negative electricity center Zn^- surrounded by one hole is caused owing to the fact that Zn atoms substitute for Fe atoms. As a result, the acceptor level is formed. The binding energy between electronegativity ion and positive hole is weak. So, valence electron is easily excited to full up the hole of the acceptor level under the light irradiation. At the same time, free hole carrier is formed due to leaving hole from ionized electron on the valence band. The acceptor level, close to the top of valence band (VB), is just like a

springboard located between valence band and conduct band. So, valence electron can be step transmitted and the energy level of each step transition is less than E_g (Energy gap) of undoped $LaFeO_3$, which is equivalent to reducing E_g value of the compound, in other words, expanding the range of photoresponse [23]. Carrier concentration increases with Zn-doped amount, which gives rise to the increase of the photocatalytic activity of $LaFeO_3$.

Second, the substitution of Zn^{2+} for Fe^{3+} is also likely due to the transformation from Fe^{3+} to Fe^{2+} due to charge compensation. Metastable Fe^{2+} ion is easy to be oxidized to form oxygen vacancy in the structure of perovskite-type [24]. Hence, Zn-doped $LaFeO_3$ exhibits enhanced redox reaction ability.

Finally, Zn occupies iron site of FeO_6 octahedral, thus leading to the change of bond angle and bond length. On the other hand, Fe–O binding energy will decrease. It is favorable for the formation of more oxygen vacancy traps on the surface of the photocatalyst. So, the photocatalytic activity of $LaFeO_3$ can be greatly improved.

However, the photocatalytic activity declines with the further increase of doping amount. The reason is that the large doping amount of Zn is more likely to serve as recombination centers than as trap sites for charge transfer at the interface. So, there is an optimum Zn-doped concentration for highest photocatalytic activity, which can be demonstrated by the XRD results (shown in Table 1). Zn inhibited the further grain growth. The restrained degree for the grain growth has a certain effect on the photocatalytic activity. Such phenomenon was also reported by Zhang et al. [25].

Conclusion

Zn-doped $LaFeO_3$ photocatalysts were prepared successfully by sol–gel auto-combustion. The crystal cells expand owing to the substitution of Zn for Fe, which result in the distortion of lattice. $LaFe_{1-x}Zn_xO_3$(x = 0, 0.05, 0.1, 0.3, 0.5)samples show a cubic perovskite structure with space group *Pm3m* (221). The absorption edges of Zn-doped $LaFeO_3$ display a red shift with a significant absorption between 400 and 500 nm. The experimental results show that the low concentration of Zn doping can significantly increase the photocatalytic activity of $LaFeO_3$ crystals. The $LaFe_{0.7}Zn_{0.3}O_3$ particles are spherical with mean grain size of about 20–30 nm, which exhibits the highest degradation rate of 75% for light time of 150 min. Due to its enhanced photocatalytic activities, this photocatalyst could be used in industrial organic wastes removal.

Acknowledgements The authors are grateful to Yongzhi Wang for performing the XRD measurements, Liu Feng for performing the SEM measurements, Shandong ceramic basic complex materials research center for financial supports, and Dr. Yujun Bai's support and help.

References

1. Li S, Jing L, Fu W, Yang L, Xin B, Fu H (2007) Mater Res Bull 42:203
2. Randeniya LK, Murphy AB, Plumb IC (2008) J Mater Sci 43:1389. doi:10.1007/s10853-007-2309-z
3. Lishan J, Tong D, Qingbiao L, Yong T (2007) Catal Commun 8:963
4. Yang Y, Sun Y, Jiang Y (2006) Mater Chem Phys 96:234
5. Yin J, Zou Z, Ye J (2003) J Phys Chem B 107:61
6. Niu X, Li H, Liu G (2005) J Mol Catal A Chem 232:89
7. Tong J, Yang W, Zhu B, Cai R (2002) J Membr Sci 203:175
8. Porob DG, Maggard PA (2006) J Solid State Chem 179:1727
9. Dong S-h, Xu K-j, Liu J-c (2007) J Synth Cryst 36:433
10. Dong S-h, Tian G-s, Feng L (2008) Chin J Nonferr Met 18:1353
11. Dereń PJ, Pązik R, Stręk W, Boutinaud Ph, Mahiou R (2008) J Alloys Compd 451:595
12. Chen Y, Yuan H, Tian G, Zhang G, Feng S (2007) J Solid State Chem 180:167
13. Debnath T, Rüscher CH, Gesing TM, Koepke J, Hussain A (2008) J Solid State Chem 181:783
14. Zhang HE, Zhang BF, Wang GF, Dong XH, Gao Y (2007) J Magn Magn Mater 312:126
15. Xiao Q, Si Z, Yu Z, Qiu G (2007) Mater Sci Eng B 137:189
16. Deorsola FA, Vallauri D (2008) J Mater Sci 43:3274. doi:10.1007/s10853-008-2530-4
17. Roy PK, Bera J (2008) J Mater Process Technol 197:279
18. Lu P (2006) Basis of inorganic material science. Publisher of Wuhan University of Technology, Wuhan
19. Burton AW, Ong K, Rea T, Chan IY (2009) Microporous Mesoporous Mater 117:83
20. Zhang H, Fu X, Niu S, Xin Q (2008) J Alloys Compd 459:103
21. Ekambaram S, Iikubo Y, Kudo A (2007) J Alloys Compd 433:237
22. Huang Y, Xie Y, Fan L, Li Y, Wei Y, Lin J, Wu J (2008) Int J Hydrogen Energy 33:6432
23. Fu X-x, Yang Q-h, Sang L-x (2002) Chem J Chin Univ 23:283
24. Xu Y-L (1991) Semiconductor basis on oxides and compounds. Xi′an University of Electronic Science and Technology Press, Xi′an
25. Zhang G, Zhou J, Ding X, Hu Y, Xie J (2008) J Hazard Mater 158:287